CHEMISTRY OF MATERIALS

Communication

pubs.acs.org/cm

High Surface Area Iron Oxide Microspheres via Ultrasonic Spray Pyrolysis of Ferritin Core Analogues

John W. Overcash and Kenneth S. Suslick*

Department of Chemistry, University of Illinois at Urbana−Champaign, 600 South Mathews Avenue, Urbana, Illinois 61802, United States

Supporting Information

The controlled synthesis and fabrication of nano- and microstructured materials has received much attention over the past decade owing to the unique chemical, electrical, magnetic, and optical properties of nanoscaled materials when compared to the bulk. Due to its low price and abundance, low toxicity, biodegradability, and high chemical stability, iron oxide is an especially promising material which has been studied for use in applications such as photocatalysis,[1−6] heavy metal removal,[7,8] sensing,[9−11] and energy storage.[4,10−14]

Previously, high surface area, nanostructured iron oxides have been synthesized by using a template, such as polystyrene microspheres[15] or copper nanowires,[16] on which iron oxide or an iron oxide precursor is grown. These templates can be expensive and are typically destroyed upon removal. Forced hydrolysis of an iron precursor in the presence of surfactants can also lead to nano- or microspheres of iron oxide with varying surface areas.[17,18] Iron oxide nanodiscs have been made using a controlled etching with oxalic acid.[19] The most common method for producing iron oxide microspheres has been solvothermal.[6,7,9,20−26] Some of these procedures require harsh chemicals or expensive surfactants, while other try to minimize the environmental impact of production. All, however, are batch processes that take many days in a high pressure vessel and generally require further workup; in addition, all of these methods are expensive (often prohibitively) and are difficult to scale-up.

Spray pyrolysis and similar aerosol techniques are well-known as scalable synthetic methodologies for the preparation of metal oxide materials from relatively inexpensive precursors.[27−32] Porous particles with relatively high surface areas have been obtained with spray pyrolysis for carbon,[33−40] silica,[41,42] titania,[43] alumina,[44] Bi_2WO_6,[45] Mn_3O_4,[46] ZnS,[47] and MoS_2.[48] Iron oxides, however, have not been previously prepared in high surface area form through spray pyrolysis; only films[49,50] and solid particles[28,51−54] have been reported.

In this work, we show the use of ultrasonic spray pyrolysis (USP)[31,32] to create very high surface area, porous, iron oxide microspheres. Through the use of colloidal oxy/hydroxy-iron(III) polymers in the precursor solution (ferritin core analogues, so-called Spiro-Saltman balls[55,56]), porous iron oxide spheres are created that are more crystalline than those made from simpler iron salt precursors. Due to the nature of USP, the size of the particles can be controlled without affecting the properties of the material; the morphology and surface area can be easily tuned by changing the salts used to prepare the precursor. This method is an inexpensive and facile way to synthesize high surface area, porous, iron oxide microspheres from simple and inexpensive precursors using the continuous, scalable process.

First, a solution of ferritin core analogues was prepared by reacting aqueous solutions of $Fe(NO_3)_3{\cdot}(H_2O)_9$ (98%, ACS from Sigma-Aldrich) with Na_2CO_3 or $NaHCO_3$ solutions. The mixture was stirred and sonicated in a cleaning bath until no more gas evolved (<5 min); this was easily monitored visually as the initially yellow Fe^{3+} solution turned opaque and brown as CO_2 gas evolved, eventually becoming a translucent dark red. DI water was added to make a 50 mL solution.

The precursor solutions were then nebulized using a made-in-house nebulizer (1.65 MHz, ∼10 W/cm^2) connected to a quartz flow tube inside a tube furnace, as described previously.[37,38] Compressed air flowing at 1 SLPM was used as a carrier gas to carry the precursor droplets through a furnace tube at 500 °C (residence time ∼10 s). The final product was collected in a series of water bubblers and washed 3× with water to remove any remaining salt porogen. During the heating of the droplets, nitrate ions decompose quickly, forming a NaOH salt template in situ and yielding NO_x gases which act as porogens.[35] The NaOH template is removed in the water bubblers and during subsequent washings leaving highly porous iron oxide spheres.

From a precursor solution containing 0.2 M $Fe(NO_3)_3$ and 0.2 M Na_2CO_3, spheres 560 ± 180 nm in diameter are formed (Figure 1a and Supporting Information Figure S1a). TEM micrographs suggest the spheres are porous throughout (Figure 1b), and Brunauer−Emmett−Teller (BET) measurements show a surface area of 301 m^2/g and average pore radius (as determined using the Barrett−Joyner−Halenda method) of 2.1 nm. This surface area is as high as any yet recorded for an iron oxide material.

Powder X-ray diffractometry (XRD) confirms the presence of α-Fe_2O_3 with an average crystallite size of 7.1 nm (Figure 2). Elemental analysis (EA) confirms the removal of the Na (<1 wt %). As a control, particles were made from a precursor composed of only $Fe(NO_3)_3$ and different amounts of the porogen $NaNO_3$ (i.e., no Spiro-Saltman balls). Compared to the Spiro-Saltman-based spheres, the control spheres (spheres formed using $Fe(NO_3)_3$ and a neutral salt porogen $NaNO_3$) had similar surface areas but decreased crystallinity (Figure 2). Conversely, by using a strong base (NaOH) in place of the weakly basic Na_2CO_3 or $NaHCO_3$ to make the precursor

Received: February 27, 2015
Revised: April 28, 2015
Published: May 5, 2015

DOI: 10.1021/acs.chemmater.5b00766
Chem. Mater. 2015, 27, 3564−3567

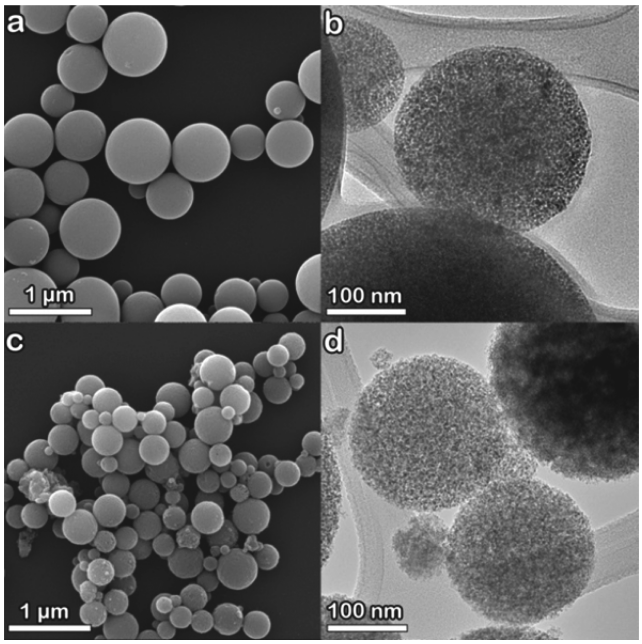

Figure 1. SEM (left) and TEM (right) micrographs of microspheres prepared from (a, b) 0.2 M $Fe(NO_3)_3$ and 0.2 M Na_2CO_3 and (c, d) 0.02 M $Fe(NO_3)_3$ and 0.02 M Na_2CO_3.

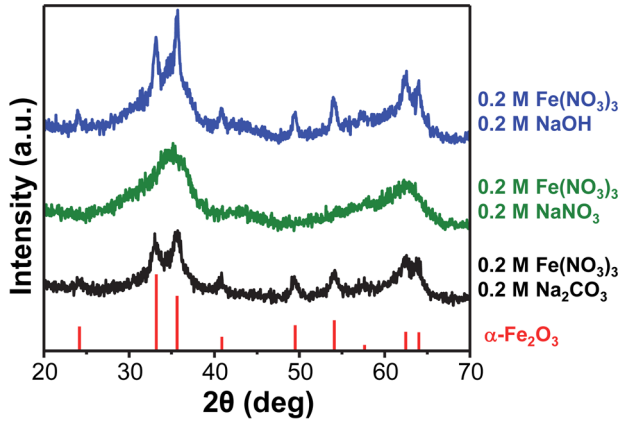

Figure 2. XRD diffractograms of the porous microspheres made from (black) Spiro-Saltman ferritin core analogues and two controls: (blue) a neutral salt and (green) a stronger base. Hematite peaks (red) are included as a reference (PDF no. 04-003-2900).

solution, larger iron oxide particles are formed resulting in relatively high crystallinity (Figure 2) but a lower surface area (206 m^2/g). The use of ferritin core analogues over simple iron salts as precursors produces products with greater crystallinity and similarly high surface areas.

The average size of the spheres is tunable by changing the concentration of the precursors. For example, spheres 280 ± 110 nm in diameter were synthesized by using 0.02 M $Fe(NO_3)_3$ and 0.02 M Na_2CO_3 (i.e., concentrations an order of magnitude smaller than that used for the original spheres) (Figure 1c and Supporting Information Figure S1b). These smaller spheres have similar properties to those of the larger spheres. Again, TEM suggests porosity throughout the entire particle (Figure 1d), and BET measurements confirm a similar surface area (294 m^2/g) and average pore radius (1.7 nm). EA confirms the removal of Na.

Other Fe^{3+} salts can also be used to prepare the Spiro-Saltman precursor. A precursor obtained by reacting $FeCl_3$ and Na_2CO_3 results in hollow, porous spheres (Figures 3e, Supporting Information Figures S2d and S3c). Here, the NaCl byproduct acts as an in situ salt template; however, unlike $NaNO_3$, no decomposition occurs, and the salt template is a solid instead of a liquid as is the case for the NaOH remaining after $NaNO_3$ decompostion (MP_{NaCl} = 801 °C and MP_{NaOH} = 318 °C).[37] The lack of the NO_x gas porogen can account for the lower surface area (97 m^2/g) of the product. Particles with intermediate morphologies and surface areas are created by simply mixing different molar ratios of $Fe(NO_3)_3$ and $FeCl_3$ (Figure 3b–d, Supporting Information Figures S2a-c and S3a-b). EA for all of the microspheres show negligible Na, indicating that the salt templates were completely removed with washing. Although the TEM for the 3:1 and 1:1 $Fe(NO_3)_3/FeCl_3$ samples appear similar to the $Fe(NO_3)_3$ only sample, the differences in surface areas indicate a decrease in porosity as more $FeCl_3$ is added. It is hypothesized that both the decrease in release of NO_x porogen and the solid salt template (NaCl) present with $FeCl_3$ rich precursors leads to larger voids.

Hematite has been suggested for use as a lithium-ion battery anode given its high capacity, environmental benignity, abundance, and low cost.[58,59] Highly porous iron oxide materials increase the practical capacity of anodes by increasing the available material for lithiation.[58,59] As a proof of concept, we tested our iron oxide microspheres as Li-ion battery anodes. Figure 4 shows the resulting charge capacities, discharge capacities, and Coulombic efficiencies for 10 cycles of a half-cell of the iron oxide-based working electrode versus a Li counter electrode for the 0.2 M $Fe(NO_3)_3$/0.2 M Na_2CO_3 spheres. As with many iron oxide anode materials, there is a very large initial charge capacity usually attributed to surface electrolyte interface layer formation.[57] The charge and discharge capacities diminish over only a few cycles and reach an ultimate efficiency

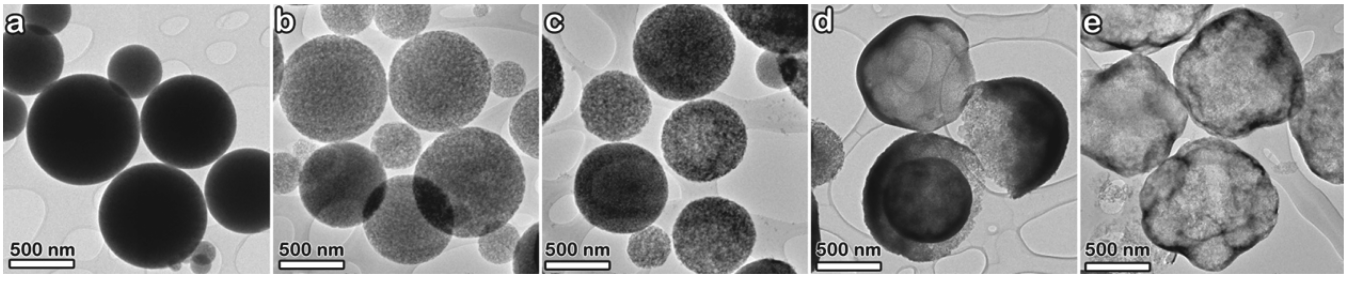

Figure 3. TEM micrographs of microspheres made from different molar ratios of $Fe(NO_3)_3/FeCl_3$: (a) $Fe(NO_3)_3$ only, (b) 3:1, (c) 1:1, (d) 1:3, and (e) $FeCl_3$ only. Scale bars are 500 nm. BET surface areas are (a) 301 m^2/g, (b) 226 m^2/g, (c) 176 m^2/g, (d) 132 m^2/g, and (e) 97 m^2/g.

DOI: 10.1021/acs.chemmater.5b00766
Chem. Mater. 2015, 27, 3564–3567

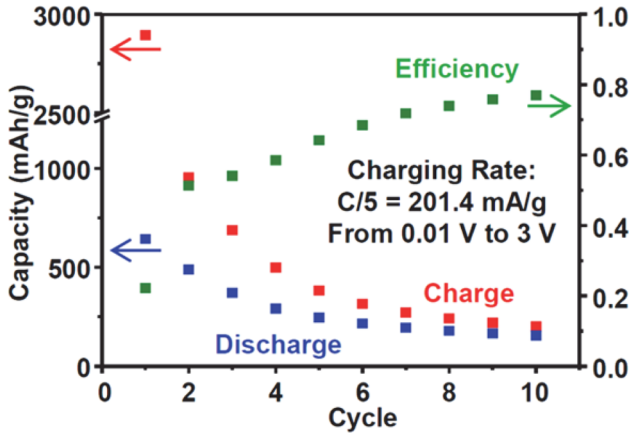

Figure 4. Charge capacity (red), discharge capacity (blue), and efficiency (green) over 10 cycles for a half-cell made with porous iron oxide from a 0.2 M $Fe(NO_3)_3$/0.2 M Na_2CO_3 precursor solution. Working electrode is 50% iron oxide, 40% conductive carbon, and 10% polyvinylidene fluoride binder by weight on a copper current collector, counter and reference electrodes are Li, and electrolyte is 1 M $LiPF_6$ in 1:1 v/v ethylene carbonate/dimethyl carbonate.

of just under 80% after 10 cycles. These results show that these materials may prove useful as anodes in lithium-ion batteries but that further development is necessary to become competitive with the current state-of-the-art.[4,58,59]

In conclusion, we have shown that highly porous iron oxide spheres of different morphologies, sizes, and crystallinities can be produced from simple and inexpensive precursors using the continuous, scalable process of ultrasonic spray pyrolysis. The nebulized precursor solution is based on colloidal iron oxy/hydroxy polymers (ferritin core analogues, so-called Spiro-Saltman balls) which allows for an increased crystallinity while maintaining a high surface area.

■ ASSOCIATED CONTENT

Supporting Information

Size distribution for Figure 1a,c; higher magnification TEM of Figure 3b−e; SEM of Figure 3b,c,e. The Supporting Information is available free of charge on the ACS Publications website at DOI: 10.1021/acs.chemmater.5b00766.

■ AUTHOR INFORMATION

Corresponding Author

*E-mail: ksuslick@illinois.edu.

Notes

The authors declare no competing financial interest.

■ ACKNOWLEDGMENTS

These studies were supported by the NSF (DMR 12-0635). Characterizations were carried out in the Center for Microanalysis of Materials at the University of Illinois at Urbana−Champaign.

■ REFERENCES

(1) Hermanek, M.; Zboril, R.; Medrik, N.; Pechousek, J.; Gregor, C. Catalytic efficiency of iron(III) oxides in decomposition of hydrogen peroxide: Competition between the surface area and crystallinity of nanoparticles. *J. Am. Chem. Soc.* **2007**, *129*, 10929−10936.

(2) Kay, A.; Cesar, I.; Gratzel, M. New benchmark for water photooxidation by nanostructured α-Fe_2O_3 films. *J. Am. Chem. Soc.* **2006**, *128*, 15714−15721.

(3) Mohapatra, S. K.; John, S. E.; Banerjee, S.; Misra, M. Water Photooxidation by Smooth and Ultrathin α-Fe_2O_3 Nanotube Arrays. *Chem. Mater.* **2009**, *21*, 3048−3055.

(4) Zhou, W.; Lin, L. J.; Wang, W. J.; Zhang, L. L.; Wu, Q. O.; Li, J. H.; Guo, L. Hierarchial Mesoporous Hematite with "Electron-Transport Channels" and Its Improved Performances in Photocatalysis and Lithium Ion Batteries. *J. Phys. Chem. C* **2011**, *115*, 7126−7133.

(5) Zhou, X. M.; Yang, H. C.; Wang, C. X.; Mao, X. B.; Wang, Y. S.; Yang, Y. L.; Liu, G. Visible Light Induced Photocatalytic Degradation of Rhodamine B on One-Dimensional Iron Oxide Particles. *J. Phys. Chem. C* **2010**, *114*, 17051−17061.

(6) Zhu, L.-P.; Bing, N.-C.; Wang, L.-L.; Jin, H.-Y.; Liao, G.-H.; Wang, L.-J. Self-assembled 3D porous flowerlike α-Fe_2O_3 hierarchical nanostructures: Synthesis, growth mechanism, and their application in photocatalysis. *Dalton Trans.* **2012**, *41*, 2959−2965.

(7) Fang, X.-L.; Chen, C.; Jin, M.-S.; Kuang, Q.; Xie, Z.-X.; Xie, S.-Y.; Huang, R.-B.; Zheng, L.-S. Single-crystal-like hematite colloidal nanocrystal clusters: synthesis and applications in gas sensors, photocatalysis and water treatment. *J. Mater. Chem.* **2009**, *19*, 6154−6160.

(8) Zeng, S.; Tang, K.; Li, T.; Liang, Z.; Wang, D.; Wang, Y.; Zhou, W. Hematite Hollow Spindles and Microspheres: Selective Synthesis, Growth Mechanisms, and Application in Lithium Ion Battery and Water Treatment. *J. Phys. Chem. C* **2007**, *111*, 10217−10225.

(9) Huang, J.; Yang, M.; Gu, C.; Zhai, M.; Sun, Y.; Liu, J. Hematite solid and hollow spindles: Selective synthesis and application in gas sensor and photocatalysis. *Mater. Res. Bull.* **2011**, *46*, 1211−1218.

(10) Sun, B.; Horvat, J.; Kim, H. S.; Kim, W.-S.; Ahn, J.; Wang, G. Synthesis of Mesoporous α-Fe_2O_3 Nanostructures for Highly Sensitive Gas Sensors and High Capacity Anode Materials in Lithium Ion Batteries. *J. Phys. Chem. C* **2010**, *114*, 18753−18761.

(11) Wu, Z.; Yu, K.; Zhang, S.; Xie, Y. Hematite Hollow Spheres with a Mesoporous Shell: Controlled Synthesis and Applications in Gas Sensor and Lithium Ion Batteries. *J. Phys. Chem. C* **2008**, *112*, 11307−11313.

(12) Brezesinski, K.; Haetge, J.; Wang, J.; Mascotto, S.; Reitz, C.; Rein, A.; Tolbert, S. H.; Perlich, J.; Dunn, B.; Brezesinski, T. Ordered Mesoporous α-Fe_2O_3 (Hematite) Thin-Film Electrodes for Application in High Rate Rechargeable Lithium Batteries. *Small* **2011**, *7*, 407−414.

(13) Liu, J.; Li, Y.; Fan, H.; Zhu, Z.; Jiang, J.; Ding, R.; Hu, Y.; Huang, X. Iron Oxide-Based Nanotube Arrays Derived from Sacrificial Template-Accelerated Hydrolysis: Large-Area Design and Reversible Lithium Storage. *Chem. Mater.* **2009**, *22*, 212−217.

(14) Poizot, P.; Laruelle, S.; Grugeon, S.; Dupont, L.; Tarascon, J. M. Nano-sized transition-metal oxides as negative-electrode materials for lithium-ion batteries. *Nature* **2000**, *407*, 496−499.

(15) Li, L.; Koshizaki, N. Vertically aligned and ordered hematite hierarchical columnar arrays for applications in field-emission, superhydrophilicity, and photocatalysis. *J. Mater. Chem.* **2010**, *20*, 2972−2978.

(16) Wang, Z. Y.; Luan, D. Y.; Madhavi, S.; Li, C. M.; Lou, X. W. α-Fe_2O_3 nanotubes with superior lithium storage capability. *Chem. Commun.* **2011**, *47*, 8061−8063.

(17) Huang, X.; Guan, J.; Xiao, Z.; Tong, G.; Mou, F.; Fan, X. a. Flower-like porous hematite nanoarchitectures achieved by complexation-mediated oxidation-hydrolysis reaction. *J. Colloid Interface Sci.* **2011**, *357*, 36−45.

(18) Tong, G.; Guan, J.; Zhang, Q. Goethite hierarchical nanostructures: Glucose-assisted synthesis, chemical conversion into hematite with excellent photocatalytic properties. *Mater. Chem. Phys.* **2011**, *127*, 371−378.

(19) Chen, J. S.; Zhu, T.; Yang, X. H.; Yang, H. G.; Lou, X. W. Top-Down Fabrication of α-Fe_2O_3 Single-Crystal Nanodiscs and Microparticles with Tunable Porosity for Largely Improved Lithium Storage Properties. *J. Am. Chem. Soc.* **2010**, *132*, 13162−13164.

(20) Pradhan, G. K.; Parida, K. M. Fabrication, Growth Mechanism, and Characterization of α-Fe_2O_3 Nanorods. *ACS Appl. Mater. Interfaces* **2011**, *3*, 317−323.

DOI: 10.1021/acs.chemmater.5b00766
Chem. Mater. 2015, 27, 3564−3567

(21) Zhu, M.; Wang, Y.; Meng, D.; Qin, X.; Diao, G. Hydrothermal Synthesis of Hematite Nanoparticles and Their Electrochemical Properties. *J. Phys. Chem. C* **2012**, *116*, 16276−16285.
(22) Bora, D. K.; Braun, A.; Erni, R.; Fortunato, G.; Graule, T.; Constable, E. C. Hydrothermal Treatment of a Hematite Film Leads to Highly Oriented Faceted Nanostructures with Enhanced Photocurrents. *Chem. Mater.* **2011**, *23*, 2051−2061.
(23) Zhu, W.; Cui, X.; Wang, L.; Liu, T.; Zhang, Q. Monodisperse porous pod-like hematite: Hydrothermal formation, optical absorbance, and magnetic properties. *Mater. Lett.* **2011**, *65*, 1003−1006.
(24) Zhang, Y. P.; Chu, Y.; Dong, L. H. One-step synthesis and properties of urchin-like PS/α-Fe_2O_3 composite hollow microspheres. *Nanotechnology* **2007**, *18*, 435608.
(25) Guo, X. H.; Deng, Y. H.; Gu, D.; Che, R. C.; Zhao, D. Y. Synthesis and microwave absorption of uniform hematite nanoparticles and their core-shell mesoporous silica nanocomposites. *J. Mater. Chem.* **2009**, *19*, 6706−6712.
(26) Kim, H.-J.; Choi, K.-I.; Pan, A.; Kim, I.-D.; Kim, H.-R.; Kim, K.-M.; Na, C. W.; Cao, G.; Lee, J.-H. Template-free solvothermal synthesis of hollow hematite spheres and their applications in gas sensors and Li-ion batteries. *J. Mater. Chem.* **2011**, *21*, 6549−6555.
(27) Okuyama, K.; Wuled Lenggoro, I. Preparation of nanoparticles via spray route. *Chem. Eng. Sci.* **2003**, *58*, 537−547.
(28) Jain, S.; Skamser, D. J.; Kodas, T. T. Morphology of Single-Component Particles Produced by Spray Pyrolysis. *Aerosol Sci. Technol.* **1997**, *27*, 575−590.
(29) Kodas, T. T.; Hampden-Smith, M. J. *Aerosol Processing of Materials*; Wiley-VCH: New York, 1999.
(30) Messing, G. L.; Zhang, S.-C.; Jayanthi, G. V. Ceramic Powder Synthesis by Spray Pyrolysis. *J. Am. Ceram. Soc.* **1993**, *76*, 2707−2726.
(31) Bang, J. H.; Suslick, K. S. Applications of Ultrasound to the Synthesis of Nanostructured Materials. *Adv. Mater.* **2010**, *22*, 1039−1059.
(32) Xu, H.; Zeiger, B. W.; Suslick, K. S. Sonochemical synthesis of nanomaterials. *Chem. Soc. Rev.* **2013**, *42*, 2555−2567.
(33) Skrabalak, S. E.; Suslick, K. S. Carbon Powders Prepared by Ultrasonic Spray Pyrolysis of Substituted Alkali Benzoates. *J. Phys. Chem. C* **2007**, *111*, 17807−17811.
(34) Skrabalak, S. E.; Suslick, K. S. Porous Carbon Powders Prepared by Ultrasonic Spray Pyrolysis. *J. Am. Chem. Soc.* **2006**, *128*, 12642−12643.
(35) Atkinson, J. D.; Fortunato, M. E.; Dastgheib, S. A.; Rostam-Abadi, M.; Rood, M. J.; Suslick, K. S. Synthesis and characterization of iron-impregnated porous carbon spheres prepared by ultrasonic spray pyrolysis. *Carbon* **2011**, *49*, 587−598.
(36) Jokić, B.; Drmanić, S.; Radetic, T.; Krstić, J.; Petrović, R.; Orlović, A.; Janaćković, D. Synthesis of submicron carbon spheres by the ultrasonic spray pyrolysis method. *Mater. Lett.* **2010**, *64*, 2173−2176.
(37) Fortunato, M. E.; Rostam-Abadi, M.; Suslick, K. S. Nanostructured Carbons Prepared by Ultrasonic Spray Pyrolysis. *Chem. Mater.* **2010**, *22*, 1610−1612.
(38) Guo, J.; Suslick, K. S. Gold nanoparticles encapsulated in porous carbon. *Chem. Commun.* **2012**, *48*, 11094−11096.
(39) Xu, H.; Guo, J.; Suslick, K. S. Porous Carbon Nanostructures: Porous Carbon Spheres from Energetic Carbon Precursors using Ultrasonic Spray Pyrolysis. *Adv. Mater.* **2012**, *24*, 6114−6114.
(40) Xu, H.; Guo, J.; Suslick, K. S. Porous Carbon Spheres from Energetic Carbon Precursors using Ultrasonic Spray Pyrolysis. *Adv. Mater.* **2012**, *24*, 6028−6033.
(41) Suh, W. H.; Suslick, K. S. Magnetic and Porous Nanospheres from Ultrasonic Spray Pyrolysis. *J. Am. Chem. Soc.* **2005**, *127*, 12007−12010.
(42) Peterson, A. K.; Morgan, D. G.; Skrabalak, S. E. Aerosol Synthesis of Porous Particles Using Simple Salts as a Pore Template. *Langmuir* **2010**, *26*, 8804−8809.
(43) Suh, W. H.; Jang, A. R.; Suh, Y. H.; Suslick, K. S. Porous, Hollow, and Ball-in-Ball Metal Oxide Microspheres: Preparation, Endocytosis, and Cytotoxicity. *Adv. Mater.* **2006**, *18*, 1832−1837.
(44) Kim, S. H.; Liu, B. Y. H.; Zachariah, M. R. Synthesis of Nanoporous Metal Oxide Particles by a New Inorganic Matrix Spray Pyrolysis Method. *Chem. Mater.* **2002**, *14*, 2889−2899.
(45) Huang, Y.; Ai, Z.; Ho, W.; Chen, M.; Lee, S. Ultrasonic Spray Pyrolysis Synthesis of Porous Bi_2WO_6 Microspheres and Their Visible-Light-Induced Photocatalytic Removal of NO. *J. Phys. Chem. C* **2010**, *114*, 6342−6349.
(46) Konstantinov, K.; Tournayre, Y.; Liu, H. K. In-situ fabrication and characterisation of nanostructured Mn_3O_4 powders for electronic and electrochemical applications. *Mater. Lett.* **2007**, *61*, 3189−3192.
(47) Bang, J. H.; Helmich, R. J.; Suslick, K. S. Nanostructured ZnS:Ni2+ Photocatalysts Prepared by Ultrasonic Spray Pyrolysis. *Adv. Mater.* **2008**, *20*, 2599−2603.
(48) Skrabalak, S. E.; Suslick, K. S. Porous MoS_2 Synthesized by Ultrasonic Spray Pyrolysis. *J. Am. Chem. Soc.* **2005**, *127*, 9990−9991.
(49) Qian, Y. T.; Niu, C. M.; Hannigan, C.; Yang, S.; Dwight, K.; Wold, A. Preparation and characterization of iron(III) oxide films by a novel spray pyrolysis method. *J. Solid State Chem.* **1991**, *92*, 208−212.
(50) García-Lobato, M. A.; Hernández-V, A.; Hdz-García, H. M.; Martínez, A. I.; Pech-Canul, M. I. Fe_2O_3 Thin Films Prepared by Ultrasonic Spray Pyrolysis. *Mater. Sci. Forum* **2010**, *644*, 105−108.
(51) Ramamurthi, M.; Leong, K. H. Generation of monodisperse metallic, metal oxide and carbon aerosols. *J. Aerosol Sci.* **1987**, *18*, 175−191.
(52) González-Carreño, T.; Morales, M. P.; Gracia, M.; Serna, C. J. Preparation of uniform γ-Fe_2O_3 particles with nanometer size by spray pyrolysis. *Mater. Lett.* **1993**, *18*, 151−155.
(53) Tang, Z. X.; Nafis, S.; Sorensen, C. M.; Hadjipanayis, G. C.; Klabunde, K. J. Magnetic properties of aerosol synthesized iron oxide particles. *J. Magn. Magn. Mater.* **1989**, *80*, 285−289.
(54) Marques, R. F. C.; Rodriguez, A. F. R.; Coaquira, J. A. H.; Santos, J. G.; Garg, V. K.; Jafelicci, M., Jr.; Ribeiro, S. J. L.; Verelst, M.; Dexpert-Ghys, J.; Morais, P. C. Mössbauer spectroscopy study of iron oxide nanoparticles obtained by spray pyrolysis. *Hyperfine Interact.* **2009**, *189*, 159−166.
(55) Brady, G. W.; Kurkjian, C. R.; Lyden, E. F. X.; Robin, M. B.; Saltman, P.; Spiro, T.; Terzis, A. Structure of an Iron Core Analog of Ferritin. *Biochemistry* **1968**, *7*, 2185−2192.
(56) Spiro, T. G.; Allerton, S. E.; Renner, J.; Terzis, A.; Bils, R.; Saltman, P. Hydrolytic Polymerization of Iron(III). *J. Am. Chem. Soc.* **1966**, *88*, 2721−2726.
(57) Larcher, D.; Masquelier, C.; Bonnin, D.; Chabre, Y.; Masson, V.; Leriche, J. B.; Tarascon, J. M. Effect of Particle Size on Lithium Intercalation into α-Fe_2O_3. *J. Electrochem. Soc.* **2003**, *150*, A133−A139.
(58) Goriparti, S.; Miele, E.; De Angelis, F.; Di Fabrizio, E.; Proietti Zaccaria, R.; Capiglia, C. Review on recent progress of nanostructured anode materials for Li-ion batteries. *J. Power Sources* **2014**, *257*, 421−443.
(59) Zheng, X.; Li, J. A review of research on hematite as anode material for lithium-ion batteries. *Ionics* **2014**, *20*, 1651−1663.

DOI: 10.1021/acs.chemmater.5b00766
Chem. Mater. 2015, 27, 3564−3567